

Mesoscale Dynamics in Melts of Single-Chain Polymeric Nanoparticles

Arantxa Arbe,^{*,†,Ⓢ} Jon Rubio-Cervilla,^{†,‡} Angel Alegría,^{†,‡} Angel J. Moreno,^{†,§,Ⓢ} José A. Pomposo,^{†,‡,||} Beatriz Robles-Hernández,[§] Paula Malo de Molina,^{§,∇} Peter Fouquet,[⊥] Fanni Juranyi,[#] and Juan Colmenero^{†,‡,§}

[†]Centro de Física de Materiales (CFM) (CSIC-UPV/EHU)-Materials Physics Center (MPC), Paseo Manuel de Lardizabal 5, E-20018 San Sebastián, Spain

[‡]Departamento de Física de Materiales (UPV/EHU), Apartado 1072, 20080 San Sebastián, Spain

[§]Donostia International Physics Center (DIPC), Paseo Manuel de Lardizabal 4, E-20018 San Sebastián, Spain

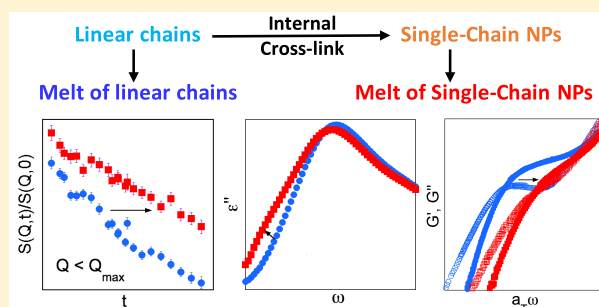
^{||}IKERBASQUE-Basque Foundation for Science, María Díaz de Haro 3, 48013 Bilbao, Spain

[⊥]Institut Laue–Langevin, BP 156, 38042 Grenoble Cedex 9, France

[#]Laboratory for Neutron Scattering, Paul Scherrer Institut, CH-5232 Villigen, Switzerland

Supporting Information

ABSTRACT: Through a combination of neutron scattering, dielectric spectroscopy, and rheological measurements we study the impact of purely intramolecular cross-linking on a melt fully made of polymeric single-chain nanoparticles (SCNPs)—a novel class of ultrasoft nano-objects. While the α -relaxation is unaffected with respect to the reference melt of linear chains, the emerging polymer/colloid duality of SCNPs leads to the almost complete smearing out of the rubbery plateau. This is the opposite effect to the creation of a permanent 3D network by intermolecular bonds. In addition, neutron scattering shows that a new relaxation mechanism slower than the α -relaxation appears at intermediate length scales. These are beyond the interchain distance but yet far from the hydrodynamic regime. This new slow relaxation—also detected by dielectric spectroscopy—contributes to the hierarchy of processes needed for the full relaxation of the SCNP melt and is tentatively related to the heterogeneities provoked by the internal multiloop topology of the SCNPs and the segregation of their internal domains.



INTRODUCTION

The chance discovery of vulcanization by Goodyear in 1839 probably constituted the most revolutionary event in the history of polymer industry. In this process, creation of a relatively small amount of intermolecular cross-links between different macromolecules leads to a permanent 3-D network with an associated spectacular transformation of the macroscopic properties of the material above the glass transition, from a (peculiar) liquid to a rubber-like behavior. How does the system behave if cross-links are of purely *intramolecular* nature is an intriguing still unsolved question we are trying to answer in this work. To do that, we will consider a polymer melt only composed by so-called single-chain nanoparticles (SCNPs), which are obtained by intramolecular cross-linking of individual macromolecular chains. This system experimentally realizes the situation of a purely intramolecular cross-linked polymer bulk.

SCNPs are soft nano-objects halfway between linear chains and “standard” nanoparticles. Thanks to their ultrasoft size, softness, and internal compartmentalization they are believed

to be a fundamental ingredient in the field of nanotechnology.^{1–10} Due to their similarities with intrinsically disordered proteins (IDP)^{11,12}—ubiquitous in living organisms—SCNPs can also be used as synthetic mimics, free of specific interactions, of relevant biomacromolecules to investigate problems as important as the influence of crowding in the cellular environment. In general, studies of systems based on SCNPs allow taking a look on the still scarcely explored interface between the soft matter fields of polymers and colloids.¹³

With these ideas in mind, in this work we made a concerted effort by combining advanced chemistry and a battery of different experimental tools, including “macroscopic” (calorimetry, dielectric, and mechanical spectroscopy) and “microscopic” (neutron diffraction and neutron spin echo, NSE) techniques to study the unique properties of a SCNPs melt.

Received: June 19, 2019

Revised: August 7, 2019

Published: September 5, 2019

We employed SCNPs based on tetrahydrofuran (THF). The choice of this system obeys its availability in deuterated version,¹⁴ low glass transition temperature (T_g)—both facilitating the neutron investigation and allowing the application of different experimental techniques over a wide frequency/temperature range—and its chemical simplicity.

Neutron scattering techniques, providing spatial resolution through the scattering vector (Q) dependence of the measured magnitudes, have been applied to perdeuterated systems, to follow collective features. The comparison with a bulk sample composed by the long linear counterpart chains (precursor macromolecules without internal cross-links) demonstrates that the structure and dynamics at local length scales including the interchain distances (in particular, the structural relaxation) are hardly sensitive to intramolecular cross-links. We remind that, in general, this is also the behavior observed when the cross-links are of intermolecular nature (permanent 3D network). However, in our case, rheological experiments not only show the absence of a rubbery plateau—characteristic of a 3D network—but also a striking reduction of the transient rubber-like plateau, due to entanglements, observed in the melt of linear precursor chains. On the other hand, we were able to extend our neutron experiments to the until now almost virgin territory of the so-called intermediate length scales (ILS). The ILS region corresponds to length scales larger than the typical intermolecular (for small molecules) or interchain (for polymeric objects) distances but not yet in the hydrodynamic regime. At ILS we observe a pronounced slowdown of the collective dynamics, associated with emerging structural heterogeneities with a characteristic length of about 1 nm. Moreover, the dielectric relaxation spectra reveal an enhanced intensity in the frequency region below the α -relaxation loss peak.

The combination of the results from all of these techniques has been crucial to elaborate a consistent picture. We conclude that the local globulation and compartmentalization into domains composed by internal loops induced by the intramolecular cross-links^{11,15,16} has three main impacts: (i) introducing heterogeneities with nanometer length scale; (ii) increasing the complexity of the dynamics; in particular, a new relevant relaxation mechanism appears, presumably associated with the internal domains; and (iii) strongly hampering the formation of entanglements among macromolecules.

EXPERIMENTAL DETAILS

Materials. Tetrahydrofuran ($\geq 99.9\%$, Scharlab) and epichlorohydrin (99%, Aldrich) were dried over CaH_2 , degassed, and distilled in a vacuum line prior to use. Tris(pentafluorophenyl)borane (95%, Aldrich) was sublimed at 60 °C in a coldfinger condenser. Tetrahydrofuran- d_8 (99.5 atom % D, Acros), epichlorohydrin- d_5 (≥ 98 atom % D, Aldrich), dichloromethane (reagent grade, Aldrich), N,N -dimethylformamide ($\geq 99.8\%$, Scharlab), sodium azide ($\geq 99.5\%$, Aldrich), and methanol ($\geq 99.9\%$, Scharlab) were used as received.

Synthesis of Protonated and Deuterated Copolymers. All reactions were performed in bulk conditions under an argon atmosphere using Schlenk flasks. For the synthesis of the protonated copolymer (hCop), $\text{B}(\text{C}_6\text{F}_5)_3$ (20 mg, 0.04 mmol), tetrahydrofuran (2.50 mL, 30.8 mmol), and epichlorohydrin (0.63 mL, 8.1 mmol) were mixed in a 25 mL Schlenk flask and stirred at room temperature for 48 h. The resulting crude product was precipitated in cold methanol, yielding a sticky transparent copolymer (hCop: 1.75 g, 59% yield, $M_w = 33.4$ kg/mol, $M_w/M_n = 1.13$). The same procedure was followed for the synthesis of the deuterated sample. Hence, $\text{B}(\text{C}_6\text{F}_5)_3$ (72 mg, 0.14 mmol), tetrahydrofuran- d_8 (8.4 mL, 103 mmol), and epichlorohydrin- d_5 (1.8 mL, 23 mmol) were used to obtain the

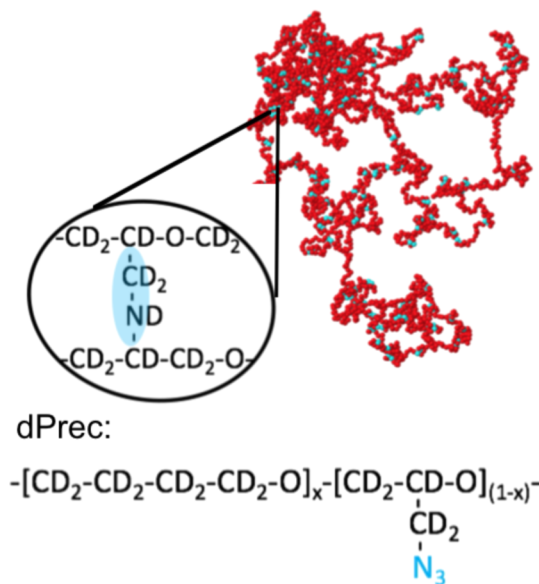
deuterated copolymer (dCop: 5.61 g, 53% yield, $M_w = 36.8$ kg/mol, $M_w/M_n = 1.23$).

Functionalization of the Protonated and Deuterated Copolymers To Obtain the Protonated and Deuterated Precursors. In a typical azidation procedure, 1.0 g of the protonated copolymer was dissolved in DMF (40 mL) in a round-bottom flask. NaN_3 (330 mg, 2 equiv) was added, and the mixture was left stirring for 24 h at 60 °C. The crude product was precipitated in a 1:1 $\text{H}_2\text{O}/\text{MeOH}$ mixture and dried under reduced pressure and at 50 °C in a vacuum oven to yield the azide-containing protonated precursor (hPrec: 0.85 g, 85% yield). The same procedure was followed to obtain the deuterated precursor (dPrec: 0.82 g, 82% yield). According to the analysis of Raman scattering bands at around 750 cm^{-1} , corresponding to C–Cl vibrations, about 30% of the chlorine atoms of the copolymer were substituted by azide groups. These results were confirmed by means of elemental analysis.

Synthesis of SCNPs from the Protonated and Deuterated Precursors. Single-chain nanoparticles (SCNPs) were synthesized via intramolecular azide photodecomposition.¹⁴ In a typical procedure, 100 mg of precursor (hPrec or dPrec) was dissolved in distilled THF (100 mL, 1 mg/mL) in a vial covered with aluminum foil and exposed to UV irradiation ($\lambda = 300\text{--}400$ nm) for 3 h at room temperature. The solvent was evaporated at reduced pressure, and the resulting product was redissolved with CH_2Cl_2 (~ 0.5 mL) and precipitated in cold methanol. SCNPs (hNP or dNP) were obtained as yellowish viscous liquids (ca. 90% yield in both cases). The final product contained about 50% of unreacted azide groups as determined by means of the analysis of the infrared absorption band at around 2100 cm^{-1} . When considering together the copolymer composition (20% mol epichlorohydrin), the substituted chlorine atoms, and the finally reacted azide groups it results that the obtained SCNPs have on average an intramolecular cross-link every 54 main-chain carbons. These results were confirmed by means of elemental analysis. The chemical formula of dPrec and the induced cross-link are shown in Scheme 1.

Relaxation Techniques. Differential scanning calorimetry (DSC) measurements were carried out on 5–10 mg of sample using a Q2000 TA Instrument. A liquid nitrogen cooling system (LCNS) was used with a 25 mL/min helium flow rate. Measurements were performed using hermetic aluminum pans. The glass transition temperatures were determined as the inflection point of the reversing heat-flow signal as recorded during cooling at 3 K/min from 373 to 173 K.

Scheme 1. MD Snapshot of a Typical SCNP in Solution^a



^aChemical formula of dPrec and a scheme of a cross-link in the real system are also shown.

Temperature-modulated experiments (MDSC) were performed using a sinusoidal variation of 0.5 K amplitude and 60 s period. The glass-transition temperatures (T_g), of 202 (hPrec) and 199 K (dPrec), increased about 1 K in the corresponding SCNPs' bulk. No signatures of crystallinity were found.

Broadband dielectric spectroscopy (BDS) experiments were conducted by using an Alpha dielectric analyzer (Novocontrol) and an E4991A RF-Impedance Analyzer (Agilent) to determine the complex dielectric permittivity ($\epsilon^*(\omega) = \epsilon'(\omega) - i\epsilon''(\omega)$) over the frequency range $f = (\omega/2\pi)$ from 10^{-2} to 10^8 Hz. Samples were placed between two flat gold-plated electrodes (10 or 20 mm diameter) forming a parallel plate capacitor with a 0.1 mm thick spacer of Teflon of negligible area between them. The temperature was controlled by a nitrogen-jet stream with a Novocontrol Quatro temperature controller. Frequency sweeps were performed at constant temperature with a stability better than 0.05 K.

Rheological experiments in the linear regime in the frequency range ≈ 0.03 –16 Hz were performed by using an ARES torsional rheometer with a parallel plate geometry (8 mm diameter) with a typical gap distance of 0.5 mm.

Neutron Scattering. With the Neutron Spin Echo (NSE) spectrometer IN11C¹⁷ at the Institute Laue Langevin (ILL) we studied the normalized dynamic structure factor $S(Q,t)/S(Q,0)$ on the deuterated samples. The scattered neutron intensity is then dominated by the coherent contribution, where all atomic pair correlations are approximately equally weighted.¹⁸ The multidetector at IN11C covers an angular range of 30° in the horizontal plane. It was placed at 20° , 50° , and 80° scattering angle for its central detector. With an incident wavelength of 5.5 Å, a Q range of $0.15 \leq Q \leq 1.64 \text{ \AA}^{-1}$ and a time range from 5 ps to 0.7 ns were explored. The experiments were performed at temperatures of 280, 320, and 360 K. To determine the resolution, a TiZi sample was used.

The structural properties were explored on the deuterated systems by small angle neutron scattering (SANS) at D11 at the ILL with an incident wavelength of 6.0 Å at 296 K. Samples were filled in quartz cuvettes (QS, Hellma) (sample thickness = 1 mm). This information was complemented at high Q values by the integrated intensity of spectra recorded by the time-of-flight FOCUS instrument¹⁹ at the Paul Scherrer Institut.

RESULTS

The structure factor $S(Q)$ —static limit of $S(Q,t)$ —presents a well-defined amorphous halo centered at around $Q_{\max} = 1.4 \text{ \AA}^{-1}$ for both linear precursor and SCNPs melts (see Figure 1a). In main-chain polymers, this peak can usually be attributed to correlations between atoms belonging to nearest neighbor chains,²⁰ separated by an average interchain distance $d \approx 2\pi/Q_{\max}$. The value $d \approx 4.5 \text{ \AA}$ is not appreciably disturbed by internal cross-links. The structural relaxation leading to the decay of these correlations is also unaltered, as shown by its characteristic time in Figure 1b and directly from the comparison of the NSE results at this Q_{\max} (squares in Figure 2). In strong contrast, the collective relaxation of SCNPs at small Q values below Q_{\max} —corresponding to the above introduced ILS region—is dramatically slowed down. This is illustrated with the results for $Q \approx 0.4 \text{ \AA}^{-1}$ shown in Figure 2. The NSE curves at different Q values were described by stretched exponentials

$$\frac{S(Q,t)}{S(Q,0)} \propto \exp\left[-\left(\frac{t}{\tau_w}\right)^\beta\right] \quad (1)$$

with values of the stretching exponent β of 0.43 (280 K), 0.47 (320 K), and 0.55 (360 K). The average characteristic times obtained as $\langle\tau\rangle = \Gamma(1/\beta)\tau_w/\beta$ are shown in Figure 1b. While in the high Q range ($Q > 0.7 \text{ \AA}^{-1}$ approx.) nearly indistinguish-

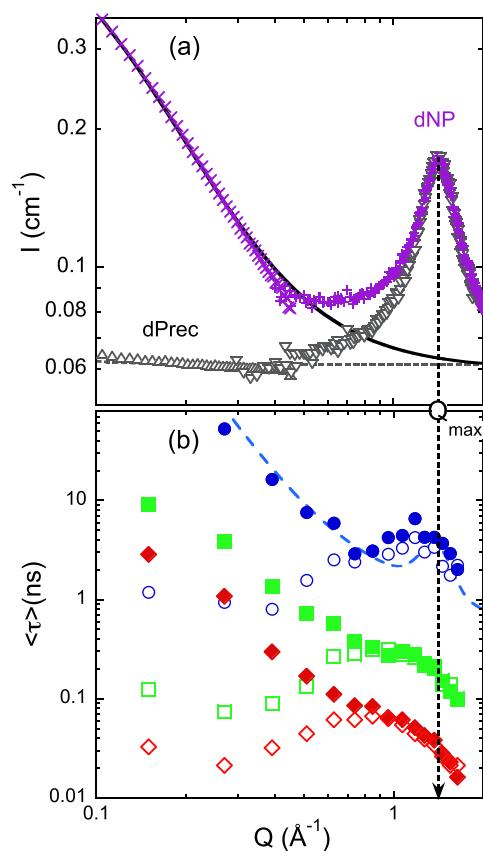


Figure 1. (a) Differential cross section of dPrec (up triangles, D11; down triangles, FOCUS) and dNP (crosses, D11; pluses, FOCUS). Dotted line marks its value for dPrec at ILS, and solid line includes an Ornstein–Zernike contribution. (b) Q dependence of the average collective characteristic times from NSE (empty symbols, dPrec; filled symbols, dNP) at 280 (circles), 320 (squares), and 360 K (diamonds). As an example, the dashed line shows the (anomalous) diffusive time for the 280 K data.²¹

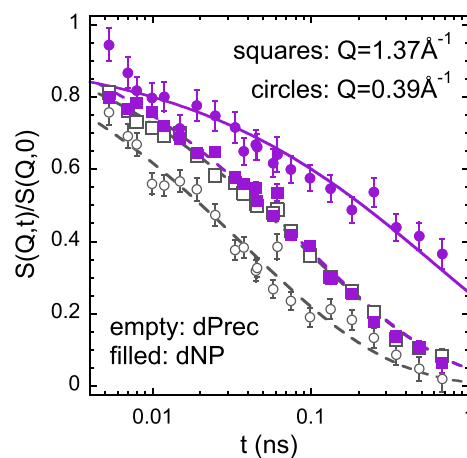


Figure 2. Normalized dynamic structure factor at $Q \approx Q_{\max}$ and a representative Q value in the ILS region at 320 K. Lines are fits of eq 1 to dPrec (dashed lines) and dNP (solid lines) data with $\beta = 0.47$.

able results can be seen for both systems, at lower Q values the collective times show an opposite behavior for SCNPs and linear chains: they tend to continuously increase toward larger length scales for the former, whereas they show an acceleration and a tendency to reach a plateau at low Q values for the latter.

This leads to a strong decoupling of the time scales of the two systems that becomes more and more acute with decreasing Q , at least in the window accessed by the present experiments.

Though the investigations of collective dynamics of glass-forming systems at ILS are still very scarce, the available experimental results^{22–24} and a recently proposed theoretical ansatz^{25,26} point to a crossover at ILS from diffusion-dominated dynamics (high Q values, covering the first structure factor peak) toward a region at low Q s where the viscoelastic coupling of stress and density fluctuations dominates. Diffusive-like mechanisms predict a kind of maximum for the characteristic time in the neighborhood of Q_{\max} —reminiscent of the deGennes narrowing²⁷—together with a continuous slowing down with decreasing Q below the Q_{\max} region. As an example, the dashed line in Figure 1b shows for $T = 280$ K the expected diffusive characteristic times deduced from incoherent scattering experiments on the protonated precursor²¹ and applying a Skögl-like renormalization, $S_{\text{coh}}(Q, t) \approx S(Q)S_{\text{inc}}(Q/\sqrt{S(Q)}, t)$.²⁸ This slowing down becomes instead an acceleration in the crossover region at ILS,²⁵ and the collective times are expected to decrease toward the value experimentally accessed by macroscopic techniques in the $Q \rightarrow 0$ limit. Such a behavior is also qualitatively found in the present results on the linear precursor melt, as can be seen in Figure 1b. The crossover would occur in the region around $Q_c \approx 0.6 \text{ \AA}^{-1}$. Beyond a certain length scale—somehow related with Q_c —the system would appear as viscoelastically homogeneous. On the contrary, the behavior of the melt of SCNPs reminds a diffusion-dominated-like dynamics in the entire Q range covered, also well below Q_{\max} (see the case of $T = 280$ K in Figure 1b). For this sample, the expected crossover to a nondiffusive characteristic time would thus be strongly shifted to low Q values (even below those accessed by the IN11C window), implying—within the proposed ansatz—that the SCNPs bulk would behave viscoelastically homogeneous only at extremely large length scales.

Structural heterogeneities responsible for such a dynamical behavior at ILS are evidenced by a pronounced increase of the low- Q scattering with respect to that in the precursor (see Figure 1a). Such an excess can be well accounted for by an Ornstein–Zernike expression,²⁹ $I_{\text{OZ}} \propto 1/[1 + (Q\xi)^2]$, with a value of $\sim 9 \text{ \AA}$ for the characteristic length ξ .

The dielectric spectroscopy (DS) results at approximately $T_g + 20$ K are shown in Figure 3. In this figure the contribution from the conductivity has been subtracted for both the precursor and the SCNP data (see full data in Figures S1 and S2 of the Supporting Information (SI)). Following the analysis explained in detail in the Appendix, the precursor data are decomposed in an α - and a β -process. These contributions can be seen as dashed–dotted lines in Figure 3. The permittivity loss peak characteristic times of the α - and β -processes in the precursor are represented in Figure 4. The DS α -relaxation times are longer than those observed by NSE at Q_{\max} , suggesting large dipolar correlations in this sample. As can be appreciated in Figure 3, internal cross-linking produces a broadening of the main loss dielectric peak, mainly affecting its low-frequency flank, and a slight apparent shift of this maximum. Since the neutron study demonstrates that the properties at local and intermolecular length scales are practically insensitive to internal cross-linking, the functional forms and characteristic times of the dielectric β - and α -

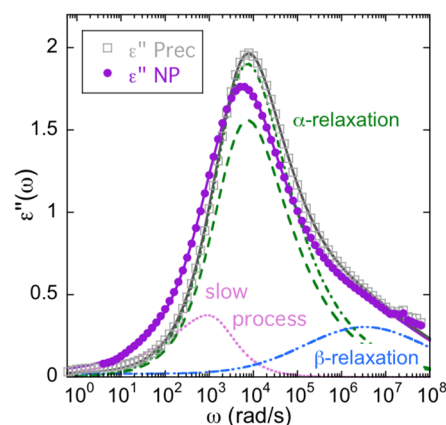


Figure 3. Dielectric losses at 220 K (conductivity subtracted). Solid lines are fitting curves considering a β -relaxation, an α -relaxation, and an additional slow contribution in the case of the SCNPs.

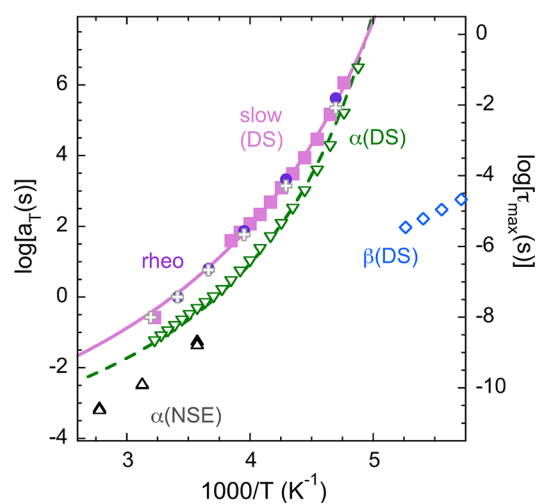


Figure 4. Relaxation map combining the rheological shift factors for precursors (empty crosses) and SCNPs (filled circles) and relaxation times (from the maxima of the imaginary part of the susceptibility function): squares, down triangles, and diamonds correspond to the slow DS, the α -process, and the β -process, respectively. Solid line shows the VFT fitting the temperature dependence of the rheological shift factors and the DS slow relaxations from the SCNPs melt. Dashed line is the VFT fit of the α -relaxation times. Up triangles show the NSE characteristic times at Q_{\max} for precursor (empty) and SCNP (filled) melts.

processes of the SCNPs can be fixed to those determined from the precursor study. However, to describe the DS results in this way we have to assume that the amplitude of the α -peak is smaller than in the SCNPs, i.e., that not all of the polarization relaxes through this process, but only a fraction x_a . Introducing the latter as a fit parameter (see Appendix), the relaxational contribution of the remaining fraction $1 - x_a$ was deduced. Figure 3 illustrates the decomposition obtained for an intermediate temperature. The additional process has a maximum at lower frequencies than the α -peak and is highly asymmetric. The temperature dependence of x_a and the shape parameter γ (see Appendix) of the low-frequency contribution are shown in Figure S3 of the SI. Except for temperatures close to T_g , the values of these parameters are independent of the temperature. From Figure S3 we conclude that the additional slow process found in the SCNPs accounts for the relaxation of

about 15% of the polarization. The temperature dependence of the characteristic time of this process is included in Figure 4. As the α -relaxation, the slower process observed in the SCNPs melt shows non-Arrhenius behavior. In both cases the description of the temperature dependence was made using a Vogel–Fulcher–Tamman (VFT) equation,^{30–32} which reads as

$$\tau(T) = \tau_{\infty} \exp\left[\frac{B}{T - T_0}\right] \quad (2)$$

We assumed the same value of the preexponential factor $\tau_{\infty} = 10^{-12}$ s for both relaxational processes. The resulting values obtained for the Vogel temperature, T_0 , and the energetic term, B , were $T_0 = 161.4$ K, $B = 1125$ K for the α -relaxation and $T_0 = 143.3$ K, $B = 1615$ K for the slower relaxation.

Moving to the rheological experiments, the master curves obtained for the real and imaginary parts of the shear modulus of the melts are presented in Figure 5. Let us first focus on the

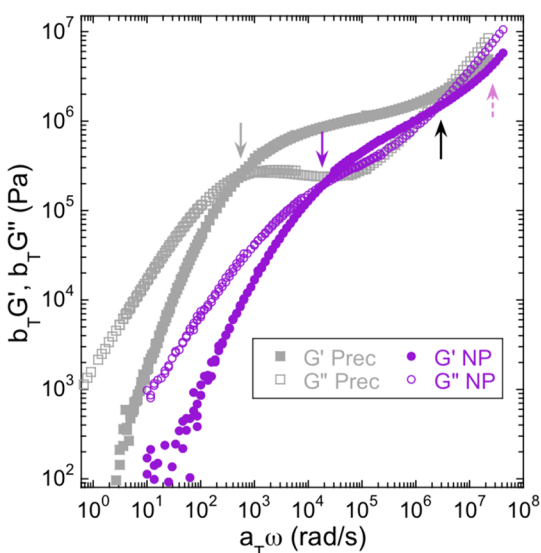


Figure 5. Rheological master curves (reference temperature 293 K). Arrows indicate the entanglement (up, solid), disentanglement (down, solid), and DS slow process (up, dotted) reduced frequencies.

linear precursor results. As it is typical for long linear chains,²⁹ these curves cross at two points: that at high frequencies reflects the onset of entanglement effects on the mechanical response, and that at low frequencies is the signature of the disentanglement of the chains. In linear polymers, the separation of these two points increases with the length of the macromolecules; in between, the reptation mechanism associated with the topological constraints imposed by neighboring chains (“entanglements”) prevails, leading to a transient “soft-solid like” behavior of the melt. The impact of intramolecular cross-linking is striking. It produces a strong shift of the low-frequency crossing point to higher frequencies, such that the plateau in the shear modulus practically disappears in the melt of SCNPs. The transient rubber-like behavior smears out, and the system readily flows. The difference with respect to the *intermolecular* cross-linking impact on the rheological properties—persistent low-frequency plateaus reflecting the permanent 3D network structure²⁹—is dramatic.

DISCUSSION

Our combined study shows that intrachain cross-linking does not change the local length scale properties (interchain average distance and dynamics of the α -relaxation) but has a strong impact at larger length scales. To provide a consistent picture of the experimental observations, we have to bear in mind that in the way SCNPs are synthesized (extremely diluted in a good solvent and with a relatively low fraction of reactive monomers in the precursors) their resulting morphology is rather sparse.^{33–35} This is illustrated by the snapshot in Scheme 1. SCNPs contain internal loops and clusters of loops (“domains”) of different sizes—but predominantly small—connected by flexible strands^{11,12,15,36} and are highly penetrable. Interpenetration of them is indeed needed to fill the space and form a melt. Structurally, intrachain cross-links manifest in the heterogeneities—extra scattering length density fluctuations—with nanometric length scale. Close to cross-links and in particular within small domains, chain conformation and packing are expected to be different than in the rest of the bulk material. Internal bonds would impose an extra constraint for relaxation of the neighboring segments, provoking retardation of the decay of density fluctuations at ILS with respect to a melt of chemically identical chains with simple linear topology. Also, the internal domain topology itself could cause certain correlations to persist over time, rendering the crossover toward a viscoelastically homogeneous regime inaccessible in the explored NSE window. Determining the characteristic length at which the crossover to viscoelastic homogeneity is reached is a crucial issue that shall be addressed with new NSE experiments, pushing the low- Q limit of the study to lower Q values. How this length compares with the correlation length estimated for the heterogeneities of about 1 nm is an intriguing open question for this kind of system. Furthermore, the single chain dynamic structure factor of the SCNPs in bulk—accessible by NSE on a melt containing some labeled protonated SCNPs in a deuterated SCNPs matrix—is a key observable that will be addressed in future experiments to provide direct insight into the loopy internal—and center of mass—dynamics of these nano-objects in the melt.

The relaxation of the internal loops could also be at the origin of the slowly relaxing fraction of the polarization, explaining the additional “slow” dielectric process. An estimation of the size of the strands participating in this process delivers lengths on the order of the nanometer, coinciding with the heterogeneity size observed by neutron scattering. The estimation of this length scale, invoking as reference the chain statistics and dynamics of the linear chains,²⁹ is as follows. The precursor entanglement relaxation time obtained from rheology at 293 K is $\tau_e(293 \text{ K}) = 2.45 \times 10^{-7}$ s. Moreover, τ_e is the relaxation time of the entanglement molecular weight M_e . This can be determined from the experimental plateau modulus $G_N = 1$ MPa, the polymer density $\rho = 1.1$ g/cm³, the gas constant $R = 8.31$ J/mol K, and the temperature $T = 293$ K as $M_e = 4\rho RT/(5G_N) \approx 2000$ g/mol. Since for molecular masses below the entanglement molecular mass Rouse dynamics would apply ($\tau \approx M^2$), we can calculate the molecular weight of the chain strands involved in a mode with characteristic time equal to that of the slow dielectric process at this temperature, $\tau_{\text{slow}}(293 \text{ K}) = 3.55 \times 10^{-8}$ s. This gives, through $\tau_{\text{slow}} = \tau_e M^2/M_e^2$, an involved mass of $M \approx 760$ g/mol. On the other hand, from SANS

experiments on a linear sample with 10% hPrec in 90% dPrec chains of $M_w = 28$ kg/mol we obtained a Gaussian form factor with average end-to-end distance $R_{ee} = 125$ Å ($R_{ee}^2/M_w = 0.556$ Å² mol/g). Taking this into account, a mass of $M \approx 760$ g/mol would correspond to an end-to-end chain strand distance of about 2 nm. Though of course this implicit mapping of the SCNP into the linear chain is a very crude approximation, it gives a rough estimation of the range of length scales involved in the slow DS process. We note that, in fact, the resulting value of 2 nm for the end-to-end chain strand distance (8 Å for the equivalent radius of gyration, assuming Gaussian statistics, $R_g^2 = 6R_{ee}^2$) is comparable with that deduced from the SANS experiments on the deuterated SCNPs melt (Ornstein–Zernike characteristic length of the heterogeneities).

In the rheological master curve the slow DS process is located close to the upper limit of the reduced frequency scale, i.e., prior to the onset of entanglements (see Figure 5). However, signatures of this process could be envisaged in the mechanical $\tan \delta$ representation. The results obtained for $\tan \delta = G''(\omega)/G'(\omega)$ for both precursor and SCNP bulks are shown in Figure 6. We note that the crossing points of the line $\tan \delta = 1$ mark the reduced frequencies corresponding to both the entanglement time (τ_e) and the disentanglement time (τ_d)²⁹ for both systems. The broadening of the low-frequency flank of the high-frequency peak is reminiscent of the

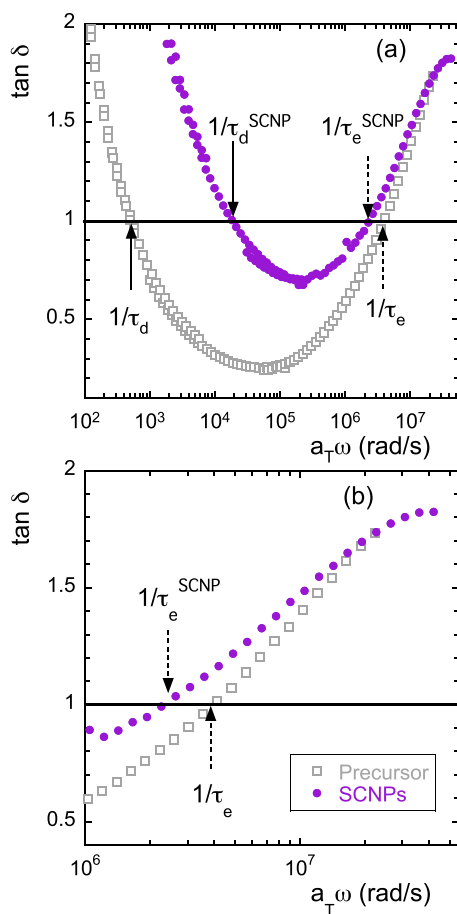


Figure 6. Reduced-frequency dependence of the $\tan \delta = G''(\omega)/G'(\omega)$ corresponding to the rheological master curves shown in Figure 5 (empty squares, precursor; filled circles, SCNPs). (a) Results in a wide frequency range, while (b) blows up of the high-frequency region.

experimental behavior observed by dielectric spectroscopy, giving rise to the slow DS process [$\tau_{\text{slow}}(293 \text{ K}) = 3.55 \times 10^{-8}$ s, i.e., its characteristic frequency is $2.8 \times 10^7 \text{ s}^{-1}$]. Then, at least qualitatively speaking, this broadening should be a mechanical signature of the dielectric slow DS process.

Accordingly, the temperature dependence of the dielectric slow process describes also well that of the shift factors used in the construction of the rheological master curves of the SCNPs (see Figure 4). This suggests that the relaxation of such newly appeared correlations associated with rigid “domains” is a prerequisite for the complete relaxation of the melt but is not directly responsible for the flow, since it takes place time decades before the disentanglement time (see Figure 5). Inspired by other architecturally complex polymer melts (stars, rings, ...), we may speculate that the flow would proceed in a highly hierarchical^{37–39} and complex way (breaking of ultrasoft cages preceded by relaxations of branches and loops); in this case, it would probably be triggered by relaxation of the heterogeneities detected by SANS and reflected in the slow DS process, which seem to be related with the internal multiloop topology.

Particular discussion is deserved by the entanglements in the system. Blurring the chain contour has a strong impact on the ability of entanglement formation. The terminal relaxation with respect to the precursor bulk is clearly accelerated, showing an “effective” reduction of entanglements. This effect is by itself relevant and highly nontrivial since, unlike dense elastic spheres, our very weakly cross-linked SCNPs are strongly interpenetrated. Again, we attribute this entanglement reduction to the presence of internal loops in the SCNPs. Macromolecular rings indeed experience much fewer contacts with other rings than their linear counterparts of the same molecular weight. This is a consequence of the topological interactions that prevent ring concatenation and lead to depletion of local domains in fractal globular structures.^{13,40,41} The entanglements reduction, linked in our case to a lower interpenetration of the chains than for the linear topology, can be considered as an indirect hint of the emergency of a soft-colloidal character in the system.

CONCLUSIONS

In summary, we presented a thorough experimental investigation of the relaxation of a melt fully made of weakly cross-linked SCNPs through a combination of scattering and relaxation techniques highly valuable to probe the complex hierarchy of dynamic processes in this system. No significant impact of intramolecular cross-linking with respect to the linear chains is found for the β - and α -relaxations. A new slow relaxation process emerges at intermediate length scales (~ 1 nm), which can be attributed to the heterogeneities provoked by the internal multiloop topology of the SCNPs. A slowly relaxing fraction of the dipolar moment also evidences the impact of internal compartmentation. Thanks to the small fraction of intramolecular cross-links present along the polymer backbone, the melt of SCNPs here investigated develops an intriguing polymer/colloid duality, where internal degrees of freedom play a key role. Due to this duality the rheological properties of this system strongly differ from those of both a 3D network (intermolecular cross-links) and a melt of long linear chains (precursors) without cross-links. Introduction of a small number of intramolecular cross-links leads to a much faster flow than in the reference linear polymer melt. This feature is tentatively assigned to the reduction of intermo-

lecular contacts (and consequently of entanglements) that originates from the characteristic segregation of intramolecular domains in dense systems of loopy objects as rings and more generally SCNPs. Our study thus nicely illustrates the essence of soft materials: “small cause, large effects”.⁴²

APPENDIX A

Analysis of DS Results

For the precursor, the relaxation curves can be described by a linear superposition of a β - and an α -process plus a power law term to account for the dc conductivity and other low-frequency effects

$$\varepsilon''(\omega) = \Delta\varepsilon_\beta \text{Im}\{\Phi_\beta^*(\omega)\} + \Delta\varepsilon_\alpha \text{Im}\{\Phi_\alpha^*(\omega)\} + \frac{A}{\omega^k} \quad (\text{A1})$$

For describing the β -relaxation we used a superposition of Debye processes with a log-normal distribution of energy barrier heights,^{43,44} which in the frequency domain reads

$$\Phi_\beta^*(\omega) = \int_0^\infty g(E) \frac{1}{1 + i\omega\tau_0 \exp\left(\frac{E}{kT}\right)} dE \quad (\text{A2})$$

where the distribution function $g(E)$ is taken as

$$g(E) = \frac{1}{\sqrt{2\pi}\sigma_E} \exp\left[-\frac{1}{2}\left(\frac{E - E_0}{\sigma_E}\right)^2\right] \quad (\text{A3})$$

Here σ_E is the width and E_0 is the average of the distribution of activation energies. The values of τ_0 and E_0 are determined from the temperature dependence of the position of the maximum of the relaxation, $\tau = \tau_0 \exp(E_0/kT)$.

Concerning the α -relaxation, we described the relaxation curves by means of the Havriliak–Negami (HN) equation⁴⁵

$$\Phi_\alpha^*(\omega) = \frac{1}{[1 + (i\omega\tau_{HN})^\alpha]^\gamma} \quad (\text{A4})$$

where τ_{HN} is the characteristic relaxation time, and the shape parameters α and γ describe respectively the symmetric and asymmetric broadening of the complex dielectric function and the condition $0 < \alpha; \alpha\beta \leq 1$ holds. We restricted ourselves to the HN-family functions which describe well the Laplace transform of Kohlrausch–Williams–Watts (KWW) functions.⁴⁶ In these cases, the relationships between HN and KWW shape parameters and their characteristic times are⁴⁶

$$\alpha\gamma = \beta^{1.23} \quad (\text{A5a})$$

$$\log\left[\frac{\tau_{HN}}{\tau_{KWW}}\right] = 2.6(1 - \beta)^{0.5} \exp(3\beta) \quad (\text{A5b})$$

The best correspondence between the HN and KWW descriptions can be found if the following relation between the HN parameters holds

$$\gamma \approx 1 - 0.8121(1 - \alpha)^{0.387} \quad (\text{A6})$$

For the SCNPs, the shape parameters and relaxation times of the β and α -processes can be fixed to those determined from the precursor analysis. To describe the DS results in this way, we have to presume that only a fraction x_a of the polarization relaxes through the α -process, thus the amplitude of the α -relaxation peak is smaller in the SCNPs. The remaining

fraction can be described by a mirrored Cole–Davidson function⁴⁷

$$\Phi_{CDm}^*(\omega) = 1 - \frac{1}{(1 + (i\omega\tau_{CD})^{-1})^\gamma} \quad (\text{A7})$$

This way, the imaginary part of the dielectric signal from the SCNPs melt is described by

$$\varepsilon''(\omega) = \Delta\varepsilon_\beta \text{Im}\{\Phi_\beta^*(\omega)\} + \Delta\varepsilon_\alpha [x_a \text{Im}\{\Phi_\alpha^*(\omega)\} + (1 - x_a) \text{Im}\{\Phi_{CDm}^*(\omega)\}] + \frac{A}{\omega^k} \quad (\text{A8})$$

where the relaxation functions of the β - and α -contributions are fixed from the precursor.

ASSOCIATED CONTENT

Supporting Information

The Supporting Information is available free of charge on the ACS Publications website at DOI: 10.1021/acs.macromol.9b01264.

Raw data and analysis of the dielectric losses of the precursor and SCNP melt; temperature dependence of the x_a and γ -parameters (PDF)

AUTHOR INFORMATION

Corresponding Author

*E-mail: a.arbe@ehu.eus. Phone: +34 943 01 8802.

ORCID

Arantxa Arbe: 0000-0002-5137-4649

Angel J. Moreno: 0000-0001-9971-0763

Present Address

[∇]Centro de Física de Materiales (CFM) (CSIC-UPV/EHU)-Materials Physics Center (MPC), Paseo Manuel de Lardizabal 5, E-20018 San Sebastián, Spain, and IKERBASQUE-Basque Foundation for Science, Maria Diaz de Haro 3, 48013 Bilbao, Spain.

Notes

The authors declare no competing financial interest.

ACKNOWLEDGMENTS

We thank Dr. S. Prévost for his help at D11. The authors gratefully acknowledge the financial support of the Basque Government, code IT-1175-19, and the Ministerio de Economía y Competitividad, code PGC2018-094548-B-I00 (MINECO/FEDER, UE). This work is based on experiments performed at the FOCUS instrument operated by the Swiss Spallation Neutron Source SINQ, Paul Scherrer Institute, Villigen, Switzerland, and has been supported by the European Commission under the seventh Framework Programme through the “Research Infrastructures” action of the “Capacities” Programme, NMI3-II Grant Number 283883.

REFERENCES

- (1) In *Single-Chain Polymer Nanoparticles: Synthesis, Characterization, Simulations, and Applications*; Pomposo, J. A., Ed.; John Wiley & Sons: Weinheim, Germany, 2017.
- (2) Kröger, A. P. P.; Paulusse, J. M. Single-chain polymer nanoparticles in controlled drug delivery and targeted imaging. *J. Controlled Release* **2018**, *286*, 326–347.

- (3) Mavila, S.; Eivgi, O.; Berkovich, I.; Lemcoff, N. G. Intra-molecular Cross-Linking Methodologies for the Synthesis of Polymer Nanoparticles. *Chem. Rev.* **2016**, *116*, 878–961.
- (4) Altintas, O.; Barner-Kowollik, C. Single-Chain Folding of Synthetic Polymers: A Critical Update. *Macromol. Rapid Commun.* **2016**, *37*, 29–46.
- (5) Latorre-Sánchez, A.; Pomposo, J. A. Recent bioinspired applications of single-chain nanoparticles. *Polym. Int.* **2016**, *65*, 855–860.
- (6) González-Burgos, M.; Latorre-Sánchez, A.; Pomposo, J. A. Advances in single chain technology. *Chem. Soc. Rev.* **2015**, *44*, 6122–6142.
- (7) Lyon, C. K.; Prasher, A.; Hanlon, A. M.; Tuten, B. T.; Tooley, C. A.; Frank, P. G.; Berda, E. B. A brief user's guide to single-chain nanoparticles. *Polym. Chem.* **2015**, *6*, 181–197.
- (8) Huo, M.; Wang, N.; Fang, T.; Sun, M.; Wei, Y.; Yuan, J. Single-chain polymer nanoparticles: Mimic the proteins. *Polymer* **2015**, *66*, A11–A21.
- (9) Pomposo, J. A. Bioinspired single-chain polymer nanoparticles. *Polym. Int.* **2014**, *63*, 589–592.
- (10) Sanchez-Sanchez, A.; Pérez-Baena, I.; Pomposo, J. A. Advances in Click Chemistry for Single-Chain Nanoparticle Construction. *Molecules* **2013**, *18*, 3339–3355.
- (11) Moreno, A. J.; Lo Verso, F.; Arbe, A.; Pomposo, J. A.; Colmenero, J. Concentrated solutions of single-chain nanoparticles: a simple model for intrinsically disordered proteins under crowding conditions. *J. Phys. Chem. Lett.* **2016**, *7*, 838–844.
- (12) Moreno, A. J.; Bacova, P.; Lo Verso, F.; Arbe, A.; Colmenero, J.; Pomposo, J. A. Effect of chain stiffness on the structure of single-chain polymer nanoparticles. *J. Phys.: Condens. Matter* **2018**, *30* (3), 034001.
- (13) Vlassopoulos, D. Macromolecular topology and rheology: beyond the tube model. *Rheol. Acta* **2016**, *55*, 613–632.
- (14) Rubio-Cervilla, J.; Malo de Molina, P.; Robles-Hernández, B.; Arbe, A.; Moreno, A. J.; Alegría, A.; Colmenero, J.; Pomposo, J. A. Facile access to completely deuterated single-chain nanoparticles enabled by intramolecular azide photodecomposition. *Macromol. Rapid Commun.* **2019**, *40* (1–6), 1900046.
- (15) Moreno, A. J.; Lo Verso, F.; Sanchez-Sanchez, A.; Arbe, A.; Colmenero, J.; Pomposo, J. A. Advantages of orthogonal folding of single polymer chains to soft nanoparticles. *Macromolecules* **2013**, *46*, 9748–9759.
- (16) Gonzalez-Burgos, M.; Arbe, A.; Moreno, A. J.; Pomposo, J. A.; Radulescu, A.; Colmenero, J. Crowding the Environment of Single-Chain Nanoparticles: A Combined Study by SANS and Simulations. *Macromolecules* **2018**, *51*, 1573–1585.
- (17) Farago, B. IN11C, medium-resolution multidetector extension of the IN11 NSE spectrometer at the ILL. *Phys. B* **1997**, *241*–243, 113–116.
- (18) Lovesey, S. W. *Theory of Neutron Scattering from Condensed Matter*; Clarendon Press: Oxford, 1984.
- (19) Jansen, S.; Mesot, J.; Holitzner, L.; Furrer, A.; Hempelmann, R. FOCUS: a hybrid TOF-sequencer at SINQ. *Physica B* **1997**, *234*–236, 1174–1176.
- (20) Frick, B.; Richter, D.; Ritter, C. Structural changes near the glass transition. *EPL (Europhysics Letters)* **1989**, *9*, 557–562.
- (21) Arbe, A.; et al. Manuscript in preparation.
- (22) Mezei, F.; Knaak, W.; Farago, B. Neutron spin echo study of dynamic correlations near liquid-glass transition. *Phys. Scr.* **1987**, *T19B*, 363–368.
- (23) Farago, B.; Arbe, A.; Colmenero, J.; Faust, R.; Buchenau, U.; Richter, D. Intermediate length scale dynamics of polyisobutylene. *Phys. Rev. E: Stat. Phys., Plasmas, Fluids, Relat. Interdiscip. Top.* **2002**, *65* (1–17), 051803.
- (24) Khairy, Y.; Alvarez, F.; Arbe, A.; Colmenero, J. Collective features in polyisobutylene. A study of the static and dynamic structure factor by molecular dynamics simulations. *Macromolecules* **2014**, *47*, 447–459.
- (25) Novikov, V. N.; Schweizer, K. S.; Sokolov, A. P. Coherent neutron scattering and collective dynamics on mesoscale. *J. Chem. Phys.* **2013**, *138* (1–6), 164508.
- (26) Colmenero, J.; Alvarez, F.; Khairy, Y.; Arbe, A. Modeling the collective relaxation time of glass-forming polymers at intermediate length scales: application to polyisobutylene. *J. Chem. Phys.* **2013**, *139* (1–6), 044906.
- (27) De Gennes, P. G. Liquid dynamics and inelastic scattering of neutrons. *Physica* **1959**, *25*, 825–839.
- (28) Sköld, K. Small Energy Transfer Scattering of Cold Neutrons from Liquid Argon. *Phys. Rev. Lett.* **1967**, *19*, 1023–1025.
- (29) Rubinstein, M.; Colby, R. H. *Polymer Physics*; Oxford University Press: Oxford, 2003.
- (30) Vogel, H. The law of the relation between the viscosity of liquids and the temperature. *Phys. Z.* **1921**, *22*, 645–646.
- (31) Fulcher, G. S. Analysis of recent measurements of the viscosity of glasses. *J. Am. Ceram. Soc.* **1925**, *8*, 339–355.
- (32) Tammann, G.; Hesse, W. Die Abhängigkeit der Viskosität von der Temperatur bei unterkühlten Flüssigkeiten. *Zeitschrift für anorganische und allgemeine Chemie* **1926**, *156*, 245–257.
- (33) Lo Verso, F.; Pomposo, J. A.; Colmenero, J.; Moreno, A. J. Multi-orthogonal folding of single polymer chains into soft nanoparticles. *Soft Matter* **2014**, *10*, 4813–4821.
- (34) Pomposo, J. A.; Perez-Baena, I.; Lo Verso, F.; Moreno, A. J.; Arbe, A.; Colmenero, J. How Far Are Single-Chain Polymer Nanoparticles in Solution from the Globular State? *ACS Macro Lett.* **2014**, *3*, 767–772.
- (35) Arbe, A.; Pomposo, J.; Moreno, A.; LoVerso, F.; González-Burgos, M.; Asenjo-Sanz, I.; Iturrospe, A.; Radulescu, A.; Ivanova, O.; Colmenero, J. Structure and dynamics of single-chain nanoparticles in solution. *Polymer* **2016**, *105*, 532–544.
- (36) Pomposo, J. A.; Moreno, A. J.; Arbe, A.; Colmenero, J. Local domain size in single-chain polymer nanoparticles. *ACS Omega* **2018**, *3*, 8648–8654.
- (37) Das, C.; Inkson, N. J.; Read, D. J.; Kelmanson, M. A.; McLeish, T. C. B. Computational linear rheology of general branch-on-branch polymers. *J. Rheol.* **2006**, *50*, 207–234.
- (38) Wang, Z.; Chen, X.; Larson, R. G. Comparing tube models for predicting the linear rheology of branched polymer melts. *J. Rheol.* **2010**, *54*, 223–260.
- (39) Ge, T.; Panyukov, S.; Rubinstein, M. Self-Similar Conformations and Dynamics in Entangled Melts and Solutions of Non-concatenated Ring Polymers. *Macromolecules* **2016**, *49*, 708–722.
- (40) Halverson, J. D.; Lee, W. B.; Grest, G. S.; Grosberg, A. Y.; Kremer, K. Molecular dynamics simulation study of nonconcatenated ring polymers in a melt. I. Statics. *J. Chem. Phys.* **2011**, *134* (1–13), 204904.
- (41) Rosa, A.; Everaers, R. Ring polymers in the melt state: the physics of crumpling. *Phys. Rev. Lett.* **2014**, *112* (1–5), 118302.
- (42) deGennes, P. G.; Badoz, J. *Fragile Objects*; Springer-Verlag, New York, 1996.
- (43) Deegan, R. D.; Nagel, S. R. Dielectric susceptibility measurements of the primary and secondary relaxation in polybutadiene. *Phys. Rev. B: Condens. Matter Mater. Phys.* **1995**, *52*, 5653–5656.
- (44) Birge, N. O.; Jeong, Y. H.; Nagel, S. R.; Bhattacharya, S.; Susman, S. Distribution of relaxation times in $(\text{KBr})_{0.5}(\text{KCN})_{0.5}$. *Phys. Rev. B: Condens. Matter Mater. Phys.* **1984**, *30*, 2306–2308.
- (45) In *Broadband Dielectric Spectroscopy*; Kremer, F., Schönhals, A., Eds.; Springer: Berlin, 2003.
- (46) Alvarez, F.; Alegría, A.; Colmenero, J. Interconnection between frequency-domain Havriliak-Negami and time-domain Kohlrausch-Williams-Watts relaxation functions. *Phys. Rev. B: Condens. Matter Mater. Phys.* **1993**, *47*, 125–130.
- (47) Böttcher, C. J. F.; Bordewijk, P. *Dielectrics in Time-Dependent Fields*; Elsevier, 1973.